

First-principles study of the anisotropic magneto-Peltier effect

Keisuke Masuda,¹ Ken-ichi Uchida,^{1,2,3,4} Ryo Iguchi,¹ and Yoshio Miura^{1,2,5}

¹Research Center for Magnetic and Spintronic Materials, National Institute for Materials Science (NIMS), Tsukuba 305-0047, Japan

²Center for Materials Research by Information Integration, National Institute for Materials Science (NIMS), Tsukuba 305-0047, Japan

³Department of Mechanical Engineering, The University of Tokyo, Tokyo 113-8656, Japan

⁴Center for Spintronics Research Network, Tohoku University, Sendai 980-8577, Japan

⁵Center for Spintronics Research Network, Osaka University, Toyonaka, Osaka 560-8531, Japan



(Received 18 June 2018; revised manuscript received 18 February 2019; published 6 March 2019)

We study theoretically the anisotropic magneto-Peltier effect, which was recently demonstrated experimentally. A first-principles-based Boltzmann transport approach including the spin-orbit interaction shows that Ni has a larger anisotropy of the Peltier coefficient ($\Delta\Pi$) than Fe, consistent with experiments. It is clarified that spin-flip electron transitions due to the spin-orbit interaction are the key in the mechanism of the large anisotropic magneto-Peltier effect. Using our method, we further predict several ferromagnetic metals with much larger $\Delta\Pi$ than that of Ni.

DOI: [10.1103/PhysRevB.99.104406](https://doi.org/10.1103/PhysRevB.99.104406)

I. INTRODUCTION

The spin-orbit interaction (SOI) plays a key role in mechanisms of various spintronic phenomena, such as the spin Hall effect [1], the Rashba–Edelstein effect [2,3], magnetic anisotropies [4], and the anisotropic magnetoresistance (AMR) [5–7]. Among them, a transport phenomenon strongly coupled with the magnetization is the AMR in ferromagnets, where the electrical resistivity depends on the relative angle between the charge current and the magnetization owing to the SOI acting on spin-polarized charge carriers.

Similar to the AMR, thermoelectric coefficients also depend on the direction of the magnetization. The Seebeck coefficient S in a ferromagnet is dependent on the relative angle between the directions of the thermal gradient ∇T and the magnetization \mathbf{M} [see Fig. 1(a)], which is called the anisotropic magneto-Seebeck effect (AMSE) [8–19]. The reciprocal effect of the AMSE called the anisotropic magneto-Peltier effect (AMPE), in which the Peltier coefficient Π depends on the relative angle between the charge current \mathbf{J}_c and \mathbf{M} , has also been investigated recently [20–22]. Uchida *et al.* [21] directly observed temperature change due to the difference in the Peltier coefficient $\Delta\Pi = \Pi_{\parallel} - \Pi_{\perp}$, where Π_{\parallel} (Π_{\perp}) is the Peltier coefficient for $\mathbf{M} \parallel \mathbf{J}_c$ ($\mathbf{M} \perp \mathbf{J}_c$) in ferromagnetic metal slabs [see Fig. 1(b)]. Uchida *et al.* [21] found that Ni, Ni₉₅Pt₅, and Ni₉₅Pd₅ exhibit clear AMPE. On the other hand, in their experiments, Fe did not show clear AMPE and Ni₄₅Fe₅₅ showed only small signals. They also observed the similar tendency in the AMSE measurements; the AMSE signal of Ni was clear but that of Fe was negligibly small [21]. Although both the AMPE (AMSE) and AMR are associated with the SOI, we can find a clear difference in the material dependence between these phenomena; while Fe exhibits the small but finite AMR [7], no clear AMPE signal was obtained in Fe in contrast with the case of Ni with a large AMPE coefficient [21]. The origin of such a strong material dependence of the AMPE and AMSE should

be clarified; however, no theoretical study has addressed the material dependence of these phenomena so far.

In this study, we investigate theoretically the intrinsic mechanism and the material dependence of the AMPE by analyzing the anisotropy of the Peltier coefficient $\Delta\Pi$ on the basis of the first-principles-based Boltzmann transport approach including the SOI. We show that $\Delta\Pi$ in Ni is much larger than that in Fe, in agreement with experimental observations, and that such a difference in $\Delta\Pi$ comes from the presence of the spin-flip electron transition around the Fermi level in Ni. Using this calculation method, we reveal that $|\Delta\Pi|$ of several ferromagnetic metal alloys containing Pt [23] is much larger than that of Ni. Although we focus only on the AMPE in this study, the results can be applied to the AMSE simply by dividing $\Delta\Pi$ by the temperature T on the basis of the Onsager reciprocal relations.

II. CALCULATION METHOD

In the present analysis, we focus on the intrinsic mechanism of the AMPE by applying the first-principles-based Boltzmann transport approach to bulk ferromagnets. This is because the AMPE (AMSE) discussed in this study occurs in bulk ferromagnets and does not require any interfaces, unlike other phenomena; e.g., the spin-dependent Seebeck and Peltier effects in magnetic nanostructures [24–26] and the magneto-Seebeck and Peltier effects in magnetic tunnel junctions [27–29].

The electronic structure of each system was calculated by using the full-potential linearized augmented plane-wave (FLAPW) method including the SOI implemented in the WIEN2K program [30]. We employed conventional unit cells for bcc Fe and fcc Ni [31], where we set \mathbf{M} along the [001] direction [see insets of Fig. 2(a)]. By applying Boltzmann transport theory [32] to the obtained electronic structures, we

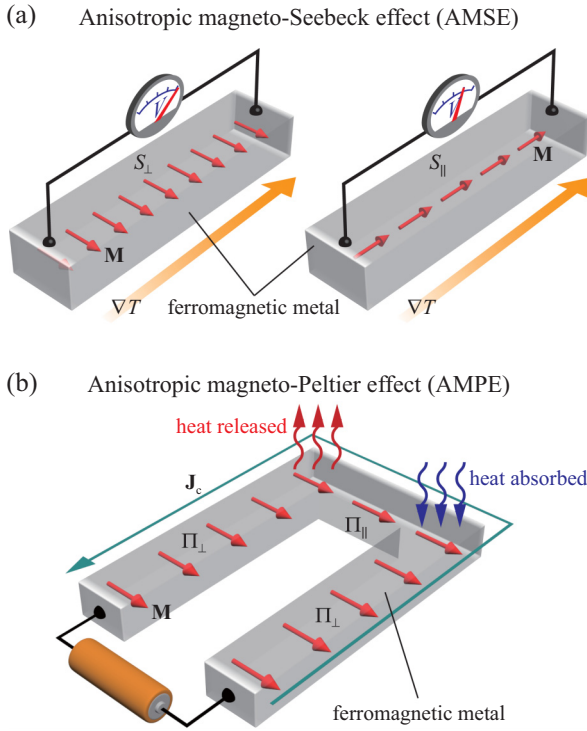


FIG. 1. Schematic illustrations of (a) the AMSE and (b) the AMPE.

calculated the Peltier coefficient Π_{α} ($\alpha = \perp, \parallel$) given by

$$\Pi_{\alpha} = -\frac{1}{e} \frac{\int \sigma_{\alpha}(\epsilon)(\epsilon - \mu) \left(-\frac{\partial f}{\partial \epsilon}\right) d\epsilon}{\int \sigma_{\alpha}(\epsilon) \left(-\frac{\partial f}{\partial \epsilon}\right) d\epsilon}, \quad (1)$$

where μ is the chemical potential, $f(\epsilon) = \{\exp[(\epsilon - \mu)/k_B T] + 1\}^{-1}$ is the Fermi distribution function, and $\sigma_{\alpha}(\epsilon) = \frac{e^2 \tau}{N} \sum_{i, \mathbf{k}} v_{\alpha}(i, \mathbf{k}) v_{\alpha}(i, \mathbf{k}) \delta(\epsilon - \epsilon_{i, \mathbf{k}})$ is the energy-dependent conductivity. Here, $\epsilon_{i, \mathbf{k}}$ is the eigenenergy with wave vector \mathbf{k} in band i , $v_{\parallel}(i, \mathbf{k})$ [$v_{\perp}(i, \mathbf{k})$] is the group velocity along the direction parallel (perpendicular) to \mathbf{M} , τ is the relaxation time assumed to be constant, and N is the number of \mathbf{k} points used in the summation. The temperature T in the Fermi function was fixed to 300 K in our analysis to compare with experiments performed at room temperature [21]. We estimated the AMPE from the anisotropy of the Peltier coefficient $\Delta \Pi \equiv \Pi_{\parallel} - \Pi_{\perp}$.

We also analyzed the AMR given by the anisotropy of the electrical resistivity. The AMR ratio is defined as $\Delta \rho / \rho_{av} = (\rho_{\parallel} - \rho_{\perp}) / (\frac{1}{3} \rho_{\parallel} + \frac{2}{3} \rho_{\perp})$, where ρ_{\parallel} (ρ_{\perp}) is the electrical resistivity when the electric current is parallel (perpendicular) to the magnetization. Note here that ρ_{α} ($\alpha = \perp, \parallel$) is the inverse of the electrical conductivity σ_{α} and is formulated as follows in Boltzmann transport approach:

$$\rho_{\alpha} = \frac{1}{\sigma_{\alpha}} = \frac{1}{\int \sigma_{\alpha}(\epsilon) \left(-\frac{\partial f}{\partial \epsilon}\right) d\epsilon}. \quad (2)$$

By comparing Eqs. (1) and (2), we see that the numerator of Eq. (1) gives the difference in the material dependence between the AMPE and AMR, which will be discussed in more detail in the next section.

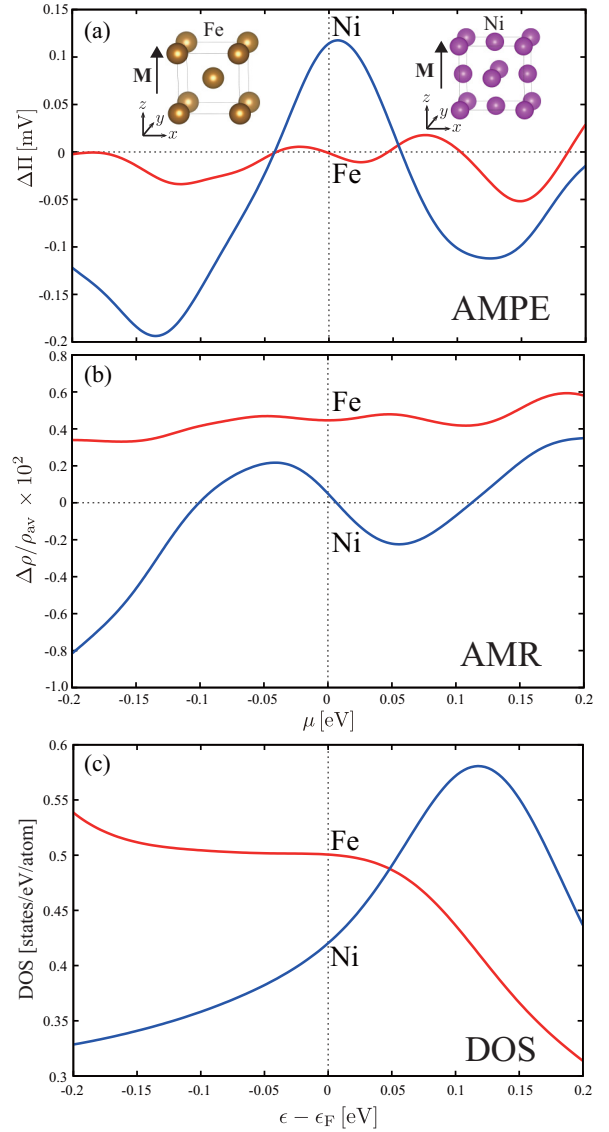


FIG. 2. Calculated μ dependencies of (a) the anisotropy of the Peltier coefficient $\Delta \Pi = \Pi_{\parallel} - \Pi_{\perp}$ and (b) the AMR ratio $\Delta \rho / \rho_{av}$ for Fe and Ni. (c) The total DOS of Fe and Ni.

III. RESULTS AND DISCUSSION

In Fig. 2(a), we show the calculated anisotropy of the Peltier coefficient $\Delta \Pi$ as a function of the chemical potential μ for Fe and Ni. Here, $\mu = 0$ corresponds to the Fermi level ϵ_F . At $\mu = 0$, Ni has a $\Delta \Pi$ of 0.114 mV, which is much larger than that of Fe [33]. These values of $\Delta \Pi$ are consistent with the experimental ones [21], not only qualitatively but also quantitatively. We also calculated the μ dependencies of AMR ratios for Fe and Ni, as shown in Fig. 2(b), where the AMR ratio of Fe is larger than that of Ni around $\mu = 0$. Such opposite material dependencies of the AMPE and AMR clearly indicate that these phenomena follow different physical pictures, consistent with the findings of previous theoretical studies [34,35].

To explain the fundamental physical properties of the Peltier coefficient, one can utilize the following approximate

expression of Eq. (1), called the Mott formula [36]:

$$\Pi \approx -\frac{\pi^2(k_B T)^2}{3e} \frac{1}{D(\epsilon_F)} \left[\frac{dD(\epsilon)}{d\epsilon} \right]_{\epsilon=\epsilon_F}, \quad (3)$$

where Π is the Peltier coefficient and $D(\epsilon)$ is the density of states (DOS). This expression suggests that a smaller $D(\epsilon_F)$ and a larger $[dD(\epsilon)/d\epsilon]_{\epsilon=\epsilon_F}$ are better for obtaining a larger Π and its anisotropy. As shown in Fig. 2(c), the DOS of Ni satisfies such conditions.

Our results for the AMR ratios can be understood from the relation that the electrical conductivity is approximately proportional to the DOS at the Fermi level $D(\epsilon_F)$, which is derived in the same manner as Eq. (3) [36]. This relation holds for the present case because we confirmed that the calculated σ_{\perp} (σ_{\parallel}) of Fe is larger than that of Ni, as expected from the DOS shown in Fig. 2(c). Owing to such a material dependence in the conductivity, the anisotropy $\sigma_{\perp} - \sigma_{\parallel}$ is also larger in Fe than in Ni, leading to the AMR ratios shown in Fig. 2(b). Note here that our calculations for the AMR ratios took into account only the intrinsic contribution from the band structures of Fe and Ni. On the other hand, in actual experiments, s - d scattering due to impurities provides non-negligible contributions to the conductivity [37], leading to the experimental behavior that the AMR ratio of Ni is larger than that of Fe [7]. However, in the case of the AMPE, not only the DOS itself but also its derivative give a large contribution to the Peltier coefficient. Therefore, in ferromagnets having a large $[dD(\epsilon)/d\epsilon]_{\epsilon=\epsilon_F}$ and a small $D(\epsilon_F)$, the effect of the s - d scattering is relatively weakened. This is a possible reason why our calculated value of $\Delta\Pi$ in Ni agrees quantitatively with the experimental results, even though the effect of the s - d scattering is disregarded and the relaxation time is assumed to be constant in the present study.

To obtain further insight into the large $\Delta\Pi$ in Ni, we focus on spectral weights $A(\mathbf{k}, \epsilon) = \sum_i \delta(\epsilon - \epsilon_{i,\mathbf{k}})$ [38] of Fe and Ni. Figures 3(a)–3(c) show the two-dimensional wave vector (k_{\perp}, k_{\parallel}) dependencies of $A(\mathbf{k}, \epsilon_F)$ in Fe at $k_x a/\pi = 0, 0.5,$ and $1,$ respectively. Here, $k_{\parallel}(\perp)$ represents the wave-vector coordinate parallel (perpendicular) to \mathbf{M} ; we set $k_{\parallel} = k_z$ and $k_{\perp} = k_y$ in the present case. Owing to the presence of the SOI, fourfold symmetry of $A(\mathbf{k}, \epsilon)$ in the (k_{\perp}, k_{\parallel}) plane is slightly broken for all k_x . This gives the anisotropy of $A(\mathbf{k}, \epsilon)$ between k_{\perp} and k_{\parallel} directions, $\Delta A(\mathbf{k}, \epsilon_F) \equiv A(k_x, k_y, k_z, \epsilon_F) - A(k_x, k_z, k_y, \epsilon_F)$, as shown in Figs. 3(d)–3(f). From Figs. 3(d) and 3(f), we see that non-negligible values of $\Delta A(\mathbf{k}, \epsilon_F)$ occur around the k_{\perp} and k_{\parallel} lines through (0,0), which can yield a finite value of $\Delta\Pi$. Figures 3(j)–3(l) show the anisotropy $\Delta A(\mathbf{k}, \epsilon_F)$ in Ni calculated from $A(\mathbf{k}, \epsilon_F)$ shown in Figs. 3(g)–3(i). We find that Ni has large values of $\Delta A(\mathbf{k}, \epsilon_F)$ especially at $k_x a/\pi = 0$ [Fig. 3(j)], which distribute broadly around the k_{\perp} and k_{\parallel} lines through (0,0). Such large and distributed $\Delta A(\mathbf{k}, \epsilon_F)$ can be the origin of the large $\Delta\Pi$ in Ni.

To clarify the reason for the difference in $\Delta A(\mathbf{k}, \epsilon_F)$ between Fe and Ni, we next analyzed the band structures along the k_{\perp} and k_{\parallel} lines through $\Gamma = (0, 0, 0)$, as shown in Figs. 4(a)–4(d). Note that these band structures are calculated for conventional unit cells introduced in Sec. II. This is why the band structures in Figs. 4(a)–4(d) are seemingly different from the well-known ones calculated for the primitive unit

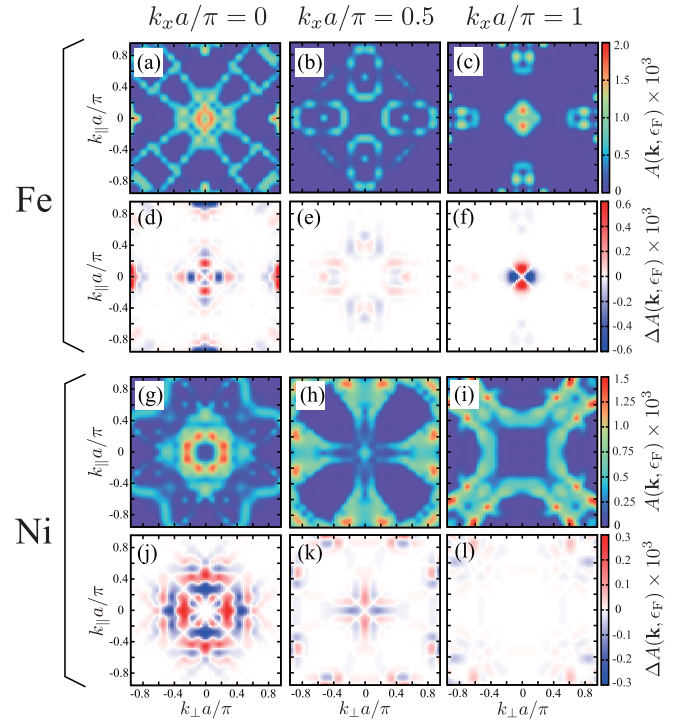


FIG. 3. (a)–(c) The in-plane wave vector (k_{\perp}, k_{\parallel}) dependencies of the spectral weight $A(\mathbf{k}, \epsilon_F)$ in Fe at (a) $k_x a/\pi = 0$, (b) $k_x a/\pi = 0.5$, and (c) $k_x a/\pi = 1$. (d)–(f) The in-plane wave vector (k_{\perp}, k_{\parallel}) dependencies of the anisotropy of the spectral weight $\Delta A(\mathbf{k}, \epsilon_F)$ in Fe at (d) $k_x a/\pi = 0$, (e) $k_x a/\pi = 0.5$, and (f) $k_x a/\pi = 1$. (g)–(i) The same as (a)–(c) for Ni. (j)–(l) The same as (d)–(f) for Ni.

cells [39,40]. The band structures for the conventional cells are identical to those obtained by folding the band structures for the primitive cells. If the SOI is absent, we can identify both majority- and minority-spin bands, which have identical dispersions in the k_{\perp} and k_{\parallel} lines [Figs. 4(a) and 4(c)]. When the SOI is taken into account, the majority- and minority-spin bands are mixed, and the k_{\perp} and k_{\parallel} lines have different band structures [Figs. 4(b) and 4(d)].

The SOI $\xi \mathbf{L} \cdot \mathbf{S} = \xi [\frac{1}{2}(L_+ S_- + L_- S_+) + L_z S_z]$ has two effects on band structures, where \mathbf{L} and \mathbf{S} are, respectively, the orbital and spin angular-momentum operators. First, the term $\frac{\xi}{2}(L_+ S_- + L_- S_+)$ gives the spin-flip electron transition between majority- and minority-spin bands, leading to the band splitting at their crossing point. In this case, the magnetic quantum numbers m in these bands need to differ with each other by 1 [41]. Second, the term $\xi L_z S_z$ gives the spin-conserving electron transition between bands with the same spin and the same m , also leading to the band splitting [42]. Since the SOI $\xi \mathbf{L} \cdot \mathbf{S}$ mainly affects the band structure along the k_{\parallel} line, this interaction gives anisotropic band structures between k_{\parallel} and k_{\perp} lines, leading to finite $\Delta A(\mathbf{k}, \epsilon_F)$.

Let us discuss each band structure of Fe and Ni in more detail. In the band structure of Fe in the absence of the SOI [Fig. 4(a)], we have a crossing point between minority-spin bands close to ϵ_F [see dashed arrow in Fig. 4(a)]. However, the band splitting due to the SOI is rather weak at this point [Fig. 4(b)]. We can also find other crossing points between the majority- and minority-spin bands, but they are not close to

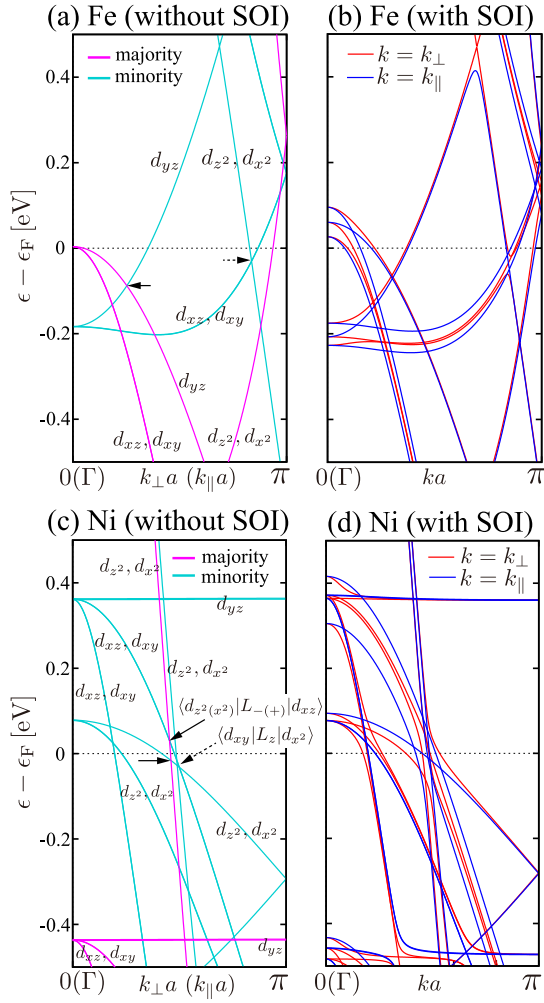


FIG. 4. Band structures along the k_{\perp} and k_{\parallel} lines through Γ for Fe in the (a) absence and (b) presence of the SOI. (c), (d) The same as (a) and (b) but for Ni. In panels (a) and (c), d orbitals contributing to each band are indicated on the curve, where $d_{3z^2-r^2}$ and $d_{x^2-y^2}$ are, respectively, abbreviated as d_{z^2} and d_{x^2} for simplicity.

ϵ_F ; the closest crossing point from ϵ_F is at $\epsilon - \epsilon_F \approx -0.09$ eV [see solid arrow in Fig. 4(a)]. Moreover, at this crossing point, since both majority- and minority-spin bands originate from the same d_{yz} state ($m = \pm 1$), the spin-flip electron transition, i.e., the band splitting, does not occur when the SOI is taken into account [Fig. 4(b)]. This is why Fe has small $\Delta A(\mathbf{k}, \epsilon_F)$. On the other hand, Ni has a favorable band structure for large $\Delta A(\mathbf{k}, \epsilon_F)$. First, near the center of the k line, three minority-spin bands cross nearly at a single point around ϵ_F [see the dashed arrow in Fig. 4(c)]. At this point, since one band includes the d_{xy} component and the other two bands have the $d_{x^2-y^2}$ component, the spin-conserving transition occurs through L_z , leading to the band splittings. Moreover, we can also find two crossing points between majority- and minority-spin bands at $\epsilon - \epsilon_F \approx 0.02$ eV and ≈ -0.01 eV, sufficiently close to ϵ_F [see the solid arrows in Fig. 4(c)]. In addition, at one of them with $\epsilon - \epsilon_F \approx 0.02$ eV, the majority-spin band comes from the $d_{3z^2-r^2}$ ($m = 0$) and $d_{x^2-y^2}$ ($m = \pm 2$) components and the minority-spin band includes the d_{xz} ($m = \pm 1$) component. Thus, at this point, the spin-flip transition

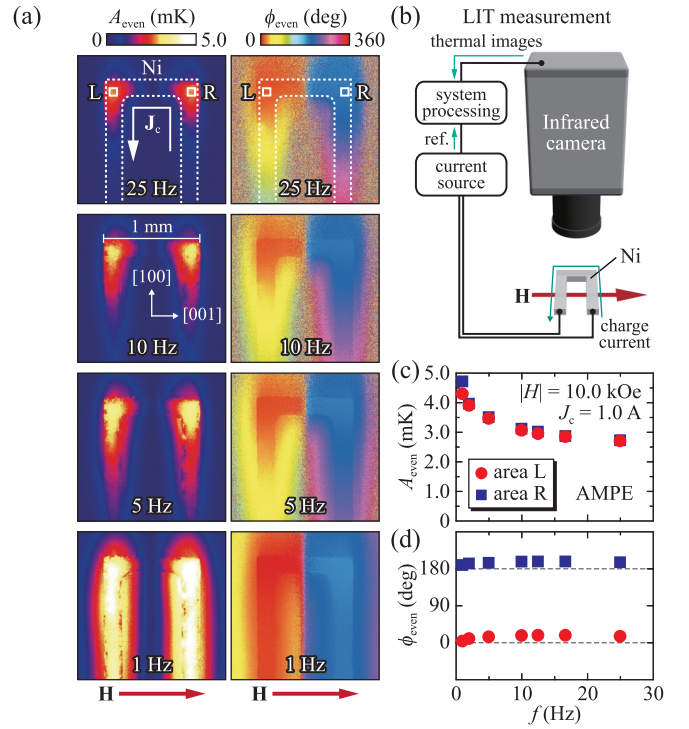


FIG. 5. Experimental results on the AMPE and AMSE in the single-crystalline Ni. (a) Lock-in amplitude A_{even} and phase ϕ_{even} images. (b) Schematic of the setup in the AMPE experiments. (c), (d) LIT frequency f dependencies of A_{even} and ϕ_{even} at the corners L and R of the U-shaped Ni sample.

occurs between the majority-spin $d_{3z^2-r^2}(x^2-y^2)$ state and the minority-spin d_{xz} state through the operator $L_{-(+)}$, leading to significant band splittings. We can conclude that, in the case of Ni, both the spin-conserving and spin-flip transitions occur around ϵ_F , which is in sharp contrast with the case of Fe with only a weak spin-conserving transition around ϵ_F . These transitions give rise to a large anisotropy of the band structure between the k_{\perp} and k_{\parallel} lines [Fig. 4(d)], which is the origin of the large $\Delta A(\mathbf{k}, \epsilon_F)$ in Ni shown in Fig. 3(j). It is well known that the exchange splitting of Ni is smaller than that of Fe [43]. This is the reason why the spin-flip transition is more effective in Ni than in Fe.

As mentioned above, our calculated value of $\Delta\Pi$ in Ni agrees with the experimental results in Ref. [21]. However, we assumed single-crystalline Ni in our calculations, although polycrystalline samples were used in the previous study. Thus, we carried out the AMPE experiments using a single-crystalline Ni for direct comparison of our theory with experiments. Using the lock-in thermography (LIT) [44–51], we observed the distribution of the temperature modulation induced by the AMPE on the surface of a U-shaped single-crystalline Ni slab with \mathbf{M} along the [001] direction. During the LIT measurements, we applied a magnetic field \mathbf{H} with magnitude $H = \pm 10.0$ kOe and a rectangularly modulated ac charge current with the amplitude of $J_c = 1.0$ A and the frequency of $f = 25.0$ Hz, and zero dc offset to the slab [Fig. 5(b)]. Since the AMPE exhibits an even dependence on the \mathbf{M} direction [21], we extract the H -even component from the raw LIT images [Fig. 5(a)], where the LIT amplitude

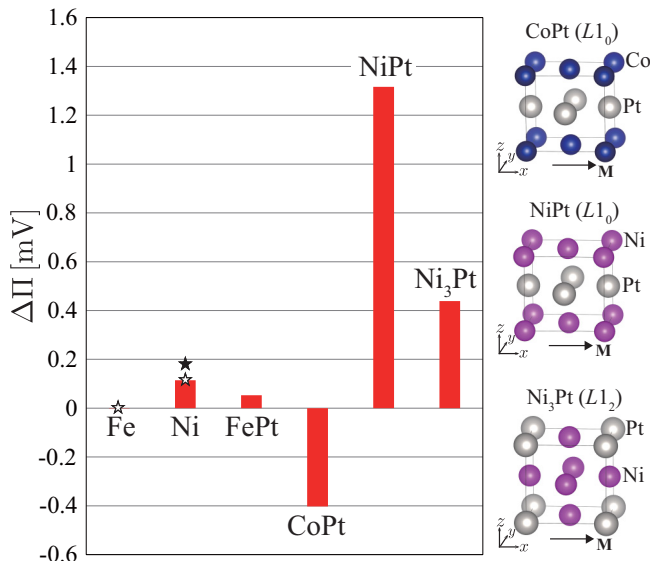


FIG. 6. Calculated values of $\Delta\Pi$ at $\mu = 0$ for Fe, Ni, FePt, CoPt, NiPt, and Ni₃Pt. White and black stars indicate experimental values estimated by the AMPE and AMSE measurements, respectively. Note that Fe does not exhibit clear AMPE in both the calculations and experiments. Crystal structures of CoPt, NiPt, and Ni₃Pt are also shown.

and phase of the H -even component are denoted by A_{even} and ϕ_{even} , respectively. As seen in the top two panels of Fig. 5(a), the signal is generated around the corners of the U-shaped structure and the sign of the temperature modulation at the corner L is opposite to that at the corner R, which is the behavior expected for the AMPE. In Figs. 5(c) and 5(d), we show the f dependencies of A_{even} and ϕ_{even} . By combining these results with numerical calculations based on finite element method [21], we obtained $\Delta\Pi = 0.11$ mV for single-crystalline Ni, which is almost the same as that for polycrystalline Ni. In Fig. 6, we compare the $\Delta\Pi$ values obtained by our calculations with those by the experiments. Here, white and black stars indicate experimental values estimated from the AMPE and AMSE measurements, respectively. We see that our theoretical values agree well with all the experimental values.

The above calculations remind us of the importance of the SOI in the mechanism of the AMPE. On the basis of this knowledge, we predict promising systems for obtaining large AMPE. We considered $L1_0$ -ordered FePt, CoPt, and NiPt, and $L1_2$ -ordered Ni₃Pt [52], since Pt has a strong SOI (Fig. 6). Here, since the [001] direction is special for the $L1_0$ structure, we set \mathbf{M} along the [100] direction and estimated $\Delta\Pi = \Pi_{\parallel} - \Pi_{\perp} = \Pi_{[100]} - \Pi_{[010]}$. We found that NiPt has a huge $\Delta\Pi$ of 1.31 mV, which is more than ten times larger than that of Ni. It was also found that CoPt and Ni₃Pt have relatively

large $|\Delta\Pi|$, which are about four times larger than that of Ni (note that CoPt has a negative $\Delta\Pi$). On the other hand, FePt has a small $\Delta\Pi$ of about half the value in Ni, although FePt is a well-known ferromagnetic metal with strong SOI. Such a nontrivial material dependence of $\Delta\Pi$ clearly indicates that not only a strong SOI but also a small exchange splitting is required for obtaining a large $\Delta\Pi$. Note that, although the largest $\Delta\Pi$ was obtained, NiPt might have a low Curie temperature ($T_C \sim 200$ K) as shown in a previous experimental study [23]. Thus, to realize huge AMPE at room temperature, CoPt ($T_C \gtrsim 800$ K) or Ni₃Pt ($T_C \gtrsim 300$ K) would be hopeful.

IV. SUMMARY

We give a microscopic physical picture of the AMPE by calculating the anisotropy of the Peltier coefficient $\Delta\Pi$ on the basis of the first-principles-based Boltzmann transport approach including the SOI. We showed that Ni has a much larger $\Delta\Pi$ than Fe, consistent with recently reported observations on polycrystalline Fe and Ni. By carrying out additional AMPE experiments using single-crystalline Ni, we confirmed that our calculated $\Delta\Pi$ also agrees with the experimental one estimated in single-crystalline Ni, which can emphasize the consistency between our theory and experiments. Analysis of the band structures clarified that the spin-flip electron transition due to the small exchange splitting is the key for the large $\Delta\Pi$ in Ni. Such an insight is important not only for advancing the understanding of the AMPE and AMSE but also for developing research for other spin-caloritronic phenomena with interconversion between charge and heat currents due to the SOI. We further calculated $\Delta\Pi$ in some ordered alloys including Pt. It was found that $L1_0$ -ordered CoPt and NiPt and $L1_2$ -ordered Ni₃Pt can have huge $|\Delta\Pi|$, which are about several to ten times larger than that of Ni. Our first-principles analysis clarified the microscopic mechanism of the AMPE and predicted hopeful materials to obtain larger AMPE, which is beneficial for developing nanoscale thermal management technologies using electronic and spintronic devices. Further experiments on the temperature dependence of the AMPE would provide more detailed information on the relationship between $\Delta\Pi$ and band structures, which will be addressed in future works.

ACKNOWLEDGMENTS

The authors are grateful to S. Mitani, M. Tsujikawa, K. Nawa, and S. Daimon for many fruitful discussions and helpful comments. This work was supported by JST-CREST ‘‘Creation of Innovative Core Technologies for Nano-enabled Thermal Management’’ (JPMJCR1711), the NEC Corporation, and NIMS MI²I. The crystal structures were visualized by using VESTA [53].

- [1] M. I. Dyakonov and V. I. Perel, *Phys. Lett. A* **35**, 459 (1971).
- [2] Y. A. Bychkov and E. I. Rashba, *JETP Lett.* **39**, 78 (1984).
- [3] V. M. Edelstein, *Solid State Commun.* **73**, 233 (1990).
- [4] B. Dieny and M. Chshiev, *Rev. Mod. Phys.* **89**, 025008 (2017).
- [5] R. M. Bozorth, *Phys. Rev.* **70**, 923 (1946).

- [6] R. Karplus and J. M. Luttinger, *Phys. Rev.* **95**, 1154 (1954).
- [7] R. T. McGuire and R. I. Potter, *IEEE Trans. Magn.* **11**, 1018 (1975).
- [8] S. R. Boona, R. C. Myers, and J. P. Heremans, *Energy Environ. Sci.* **7**, 885 (2014).

- [9] J. P. Jan, *Solid State Phys.* **5**, 1 (1957).
- [10] G. N. Grannemann and L. Berger, *Phys. Rev. B* **13**, 2072 (1976).
- [11] J.-E. Wegrowe, Q. A. Nguyen, M. Al-Barki, J.-F. Dayen, T. L. Wade, and H.-J. Drouhin, *Phys. Rev. B* **73**, 134422 (2006).
- [12] A. D. Avery, R. Sultan, D. Bassett, D. Wei, and B. L. Zink, *Phys. Rev. B* **83**, 100401(R) (2011).
- [13] R. Mittdank, M. Handwerg, C. Steinweg, W. Töllner, M. Daub, K. Nielsch, and S. F. Fischer, *J. Appl. Phys.* **111**, 104320 (2012).
- [14] A. D. Avery, M. R. Pufall, and B. L. Zink, *Phys. Rev. Lett.* **109**, 196602 (2012).
- [15] A. D. Avery, M. R. Pufall, and B. L. Zink, *Phys. Rev. B* **86**, 184408 (2012).
- [16] M. Schmid, S. Srichandan, D. Meier, T. Kuschel, J.-M. Schmalhorst, M. Vogel, G. Reiss, C. Strunk, and C. H. Back, *Phys. Rev. Lett.* **111**, 187201 (2013).
- [17] O. Reimer, D. Meier, M. Bovender, L. Helmich, J.-O. Dreessen, J. Kriefft, A. S. Shestakov, C. H. Back, J.-M. Schmalhorst, A. Hütten, G. Reiss, and T. Kuschel, *Sci. Rep.* **7**, 40586 (2017).
- [18] N. Miyata and Z. Funatogawa, *J. Phys. Soc. Jpn.* **9**, 967 (1954).
- [19] S. J. Watzman, R. A. Duine, Y. Tserkovnyak, S. R. Boona, H. Jin, A. Prakash, Y. Zheng, and J. P. Heremans, *Phys. Rev. B* **94**, 144407 (2016).
- [20] K. S. Das, F. K. Dejene, B. J. van Wees, and I. J. Vera-Marun, *Phys. Rev. B* **94**, 180403 (2016).
- [21] K. Uchida, S. Daimon, R. Iguchi, and E. Saitoh, *Nature (London)* **558**, 95 (2018).
- [22] R. Das, R. Iguchi, and K. Uchida, *Phys. Rev. Applied* (to be published); [arXiv:1809.05741](https://arxiv.org/abs/1809.05741).
- [23] C. Leroux, M. C. Cadeville, V. Pierron-Bohnes, G. Inden, and F. Hinz, *J. Phys. F: Met. Phys.* **18**, 2033 (1988).
- [24] A. Slachter, F. L. Bakker, J.-P. Adam, and B. J. van Wees, *Nat. Phys.* **6**, 879 (2010).
- [25] J. Flipse, F. L. Bakker, A. Slachter, F. K. Dejene, and B. J. van Wees, *Nat. Nanotechnol.* **7**, 166 (2012).
- [26] G. E. W. Bauer, E. Saitoh, and B. J. van Wees, *Nat. Mater.* **11**, 391 (2012).
- [27] M. Walter, J. Walowski, V. Zbarsky, M. Münzenberg, M. Schäfers, D. Ebke, G. Reiss, A. Thomas, P. Peretzki, M. Seibt, J. S. Moodera, M. Czerner, M. Bachmann, and C. Heiliger, *Nat. Mater.* **10**, 742 (2011).
- [28] J. Shan, F. K. Dejene, J. C. Leutenantsmeyer, J. Flipse, M. Münzenberg, and B. J. van Wees, *Phys. Rev. B* **92**, 020414(R) (2015).
- [29] T. Kuschel, M. Czerner, J. Walowski, A. Thomas, H. W. Schumacher, G. Reiss, C. Heiliger, and M. Münzenberg, *J. Phys. D: Appl. Phys.* **52**, 133001 (2019).
- [30] P. Blaha *et al.*, <http://www.wien2k.at>. We adopted the generalized gradient approximation for the exchange-correlation functional and used $51 \times 51 \times 51 \mathbf{k}$ points for the Brillouin-zone integration, ensuring good convergence for transport properties. The muffin-tin radii in each system were chosen as nearly touching spheres to keep as much core charges inside the muffin-tin sphere as possible.
- [31] The a -axis lengths of the cells were set to 2.86 and 3.52 Å for Fe and Ni, respectively.
- [32] We used the code named BoltzTraP, the details of which are given in Ref. [54].
- [33] The obtained $\Delta\Pi$ in Fe is negligibly small in our calculations taking into account only the electronic contribution, which is consistent with the AMPE experiments reported by Uchida *et al.* [21]. Thus, the AMSE observed in Fe under a high magnetic field [19] seems to originate from another mechanism, such as the magnon-electron interaction [55].
- [34] V. Popescu, P. Kratzer, P. Entel, C. Heiliger, M. Czerner, K. Tauber, F. Töpler, C. Herschbach, D. V. Fedorov, M. Gradhand, I. Mertig, R. Kováčik, P. Mavropoulos, D. Wortmann, S. Blügel, F. Freimuth, Y. Mokrousov, S. Wimmer, D. Ködderitzsch, M. Seemann, K. Chadova, and H. Ebert, *J. Phys. D: Appl. Phys.* **52**, 073001 (2019).
- [35] S. Wimmer, D. Ködderitzsch, and H. Ebert, *Phys. Rev. B* **89**, 161101(R) (2014).
- [36] N. W. Ashcroft and N. D. Mermin, *Solid State Physics* (Saunders College, Philadelphia, 1976).
- [37] S. Kokado, M. Tsunoda, K. Harigaya, and A. Sakuma, *J. Phys. Soc. Jpn.* **81**, 024705 (2012).
- [38] The DOS is obtained by integrating $A(\mathbf{k}, \epsilon)$ over \mathbf{k} .
- [39] J. Callaway and C. S. Wang, *Phys. Rev. B* **16**, 2095 (1977).
- [40] C. S. Wang and J. Callaway, *Phys. Rev. B* **15**, 298 (1977).
- [41] For example, the transition occurs between majority-spin bands from $d_{x^2-y^2}$ states ($m = \pm 2$) and minority-spin bands from d_{xz} states ($m = \pm 1$).
- [42] For instance, the transition occurs between majority-spin bands from d_{xz} ($m = \pm 1$) states and majority-spin bands from d_{yz} states ($m = \pm 1$).
- [43] D. E. Eastman, F. J. Himpsel, and J. A. Knapp, *Phys. Rev. Lett.* **44**, 95 (1980).
- [44] H. Straube, J.-M. Wagner, and O. Breitenstein, *Appl. Phys. Lett.* **95**, 052107 (2009).
- [45] O. Breitenstein, W. Warta, and M. Langenkamp, *Lock-in Thermography - Basics and Use for Evaluating Electronic Devices and Materials*, 2nd ed. (Springer, Berlin, 2010).
- [46] O. Wid, J. Bauer, A. Müller, O. Breitenstein, S. S. P. Parkin, and G. Schmidt, *Sci. Rep.* **6**, 28233 (2016).
- [47] S. Daimon, R. Iguchi, T. Hioki, E. Saitoh, and K. Uchida, *Nat. Commun.* **7**, 13754 (2016).
- [48] O. Wid, J. Bauer, A. Müller, O. Breitenstein, S. S. P. Parkin, and G. Schmidt, *J. Phys. D: Appl. Phys.* **50**, 134001 (2017).
- [49] K. Uchida, R. Iguchi, S. Daimon, R. Ramos, A. Anadón, I. Lucas, P. A. Algarabel, L. Morellón, M. H. Aguirre, M. R. Ibarra, and E. Saitoh, *Phys. Rev. B* **95**, 184437 (2017).
- [50] S. Daimon, K. Uchida, R. Iguchi, T. Hioki, and E. Saitoh, *Phys. Rev. B* **96**, 024424 (2017).
- [51] Y. Hirayama, R. Iguchi, X.-F. Miao, K. Hono, and K. Uchida, *Appl. Phys. Lett.* **111**, 163901 (2017).
- [52] The a -axis lengths of the conventional unit cells were set to 3.86, 3.80, 3.80, and 3.64 Å for FePt ($L1_0$), CoPt ($L1_0$), NiPt ($L1_0$), and Ni₃Pt ($L1_2$), respectively. In the systems with $L1_0$ structure, the values of c/a were fixed to 0.981, 0.973, and 0.974 for FePt, CoPt, and NiPt, respectively.
- [53] K. Momma and F. Izumi, *J. Appl. Crystallogr.* **44**, 1272 (2011).
- [54] G. K. H. Madsen and D. J. Singh, *Comput. Phys. Commun.* **175**, 67 (2006).
- [55] F. J. Blatt, D. J. Flood, V. Rowe, P. A. Schroeder, and J. E. Cox, *Phys. Rev. Lett.* **18**, 395 (1967).